Research Article

Cancer Immunology Research

Natural Killer Cell Recruitment and Activation Are Regulated by CD47 Expression in the Tumor Microenvironment

Pulak Ranjan Nath[1], Dipasmita Pal-Nath[1], Ajeet Mandal[2], Margaret C. Cam[3], Anthony L. Schwartz[1], and David D. Roberts[1]

Abstract

Elevated CD47 expression in some cancers is associated with decreased survival and limited clearance by phagocytes expressing the CD47 counterreceptor SIRPα. In contrast, elevated CD47 mRNA expression in human melanomas was associated with improved survival. Gene-expression data were analyzed to determine a potential mechanism for this apparent protective function and suggested that high CD47 expression increases recruitment of natural killer (NK) cells into the tumor microenvironment. The CD47 ligand thrombospondin-1 inhibited NK cell proliferation and CD69 expression *in vitro*. *Cd47*$^{-/-}$ NK cells correspondingly displayed augmented effector phenotypes, indicating an inhibitory function of CD47 on NK cells. Treating human NK cells with a CD47 antibody that blocks thrombospondin-1 binding abrogated its inhibitory effect on NK cell proliferation. Similarly, treating wild-type mice with a CD47 antibody that blocks thrombospondin-1 binding delayed B16 melanoma growth, associating with increased NK cell recruitment and increased granzyme B and interferon-γ levels in intratumoral NK but not CD8^{+} T cells. However, B16 melanomas grew faster in *Cd47*$^{-/-}$ than in wild-type mice. Melanoma-bearing *Cd47*$^{-/-}$ mice exhibited decreased splenic NK cell numbers, with impaired effector protein expression and elevated exhaustion markers. Proapoptotic gene expression in *Cd47*$^{-/-}$ NK cells was associated with stress-mediated increases in mitochondrial proton leak, reactive oxygen species, and apoptosis. Global gene-expression profiling in NK cells from tumor-bearing mice identified CD47-dependent transcriptional responses that regulate systemic NK activation and exhaustion. Therefore, CD47 positively and negatively regulates NK cell function, and therapeutic antibodies that block inhibitory CD47 signaling can enhance NK immune surveillance of melanomas.

Introduction

CD47 is a transmembrane protein that interacts with several integrins, two signal-regulatory protein (SIRP) family counterreceptors, and the secreted protein thrombospondin-1 (1–3). Malignant cells in some hematopoietic malignancies and solid tumors express elevated levels of CD47 relative to healthy tissues, and elevated CD47 in some cancers is correlated with poor prognosis (4). The prevailing hypothesis is that interaction of tumor cell CD47 with the counterreceptor SIRPα on macrophages inhibits phagocytosis of tumor cells (4). Conversely, antibody-mediated blockade of SIRPα binding or knockdown of CD47 promotes active phagocytosis of implanted human xenograft tumors in mice expressing a variant of SIRPα that binds human CD47 with high affinity (4, 5). In contrast, blocking SIRPα binding to CD47 is generally not sufficient to promote phagocytic clearance of syngeneic tumors in immune-competent mice, which requires additional immune stimuli to induce CD8 T cell–mediated tumor killing (4, 6, 7). CD47 is an inhibitory signaling receptor for thrombospondin-1 on T cells (8, 9). Thrombospondin-1 signaling through CD47 also inhibits antigen presentation by dendritic cells to T cells (10). CD47 is, therefore, an innate and adaptive immune checkpoint.

We found that natural killer (NK) cells express high levels of CD47 mRNA and cell-surface protein, which regulates NK cell homeostasis and their response to viral infection in mice (11). NK cells are also a first line of defense system against malignant cell transformation (12–14).

NK cell development, education, and effector functions are regulated by several families of activating and inhibitory receptors, including the killer cell immunoglobulin-like receptor (KIR) family, the CD94 family, the leukocyte immunoglobulin-like receptor (LIR) family, and NKG2D and the natural cytotoxicity receptors (NCR) NKp30, NKp44, and NKp46 (15). Inhibitory NK receptors recognize MHC class I, as well as non–MHC-I ligands such as PVR (15–19). The regulatory roles of thrombospondin-1 and CD47 in NK cells are less clear. Thrombospondin-1 inhibits early NK cell proliferation and enhances late expansion, but a role for CD47 in these activities was not examined (20). Functioning

[1]Laboratory of Pathology, Center for Cancer Research, National Cancer Institute, National Institutes of Health, Bethesda, Maryland. [2]Human Brain Collection Core, National Institute of Mental Health, National Institutes of Health, Bethesda, Maryland. [3]CCR Collaborative Bioinformatics Resource, Office of Science and Technology Resources, National Cancer Institute, and Leidos Biomedical Research, Inc., National Institutes of Health, Bethesda, Maryland.

Note: Supplementary data for this article are available at Cancer Immunology Research Online (http://cancerimmunolres.aacrjournals.org/).

Current address for P.R. Nath: The Jackson Laboratory for Genomic Medicine, Farmington, Connecticut.

Corresponding Authors: David D. Roberts, National Institutes of Health, Building 10, Room 2S235, 10 Center Drive MSC1500, Bethesda, MD 20892-1500. Phone: 301-480-4369; Fax: 301-480-0611; E-mail: droberts@mail.nih.gov; and Pulak Ranjan Nath, hellopran2000@gmail.com

Cancer Immunol Res 2019;7:1547–61

doi: 10.1158/2326-6066.CIR-18-0367

as a SIRPα counterreceptor, CD47 enables engraftment of NK precursors in mice reconstituted with a human immune system (21). Treatment with a CD47 antibody that inhibits SIRPα and thrombospondin-1 binding increased NK cell killing of head-and-neck squamous carcinoma cells *in vitro*, but the mechanism remains unclear because NK cells are not known to express SIRPα (22). Depletion of NK cells similarly attenuated the antitumor activity of a SIRPα blocking antibody in a syngeneic murine renal carcinoma model, but the same antibody did not inhibit NK killing of the tumor cells *in vitro*, suggesting a SIRPα-independent function of CD47 in NK cells (23).

Analysis of The Cancer Genome Atlas (TCGA) data for human melanomas showed positive correlations between CD47 mRNA expression and patient survival and CD47 expression with the expression of NK early activation genes. We identified CD47-dependent inhibitory functions for thrombospondin-1 in human and murine NK cells *in vitro*. Correspondingly, inhibition of melanoma growth following treatment with a CD47 antibody that inhibits thrombospondin-1 binding was associated with enhanced NK cell activation. In contrast, B16 melanoma tumors grew faster in $Cd47^{-/-}$ mice, which was associated with reduced NK frequency and enhanced NK exhaustion, similar to that observed during chronic lymphocytic choriomeningitis virus (LCMV) infection of $Cd47^{-/-}$ mice (11). Gene-expression and functional studies in NK cells identified impaired mitochondrial function and an enhanced proapoptotic signature in $Cd47^{-/-}$ NK cells when subjected to stress. Therefore, we demonstrated that CD47 has both positive and negative roles in regulating antitumor NK immunity.

Materials and Methods

Mice

Mice were maintained under specific pathogen-free conditions, and the NCI Animal Care and Use Committee approved all treatments under protocol NCI/LP-012. Breeding pairs of wild-type (WT) and B6.129S7-Cd47^{tm1Fpl}/J ($Cd47^{-/-}$) C57BL/6J mice (The Jackson Laboratory) were backcrossed to minimize genetic drift and obtain $Cd47^{+/-}$ mice. Heterozygous $Cd47^{+/-}$ were bred to obtain $Cd47^{+/+}$, $Cd47^{+/-}$, and $Cd47^{-/-}$ littermate mice. Mouse genotypes were confirmed by PCR using a set of primers targeting the mouse CD47 allele. Littermate and sex-matched mice between 6 and 12 weeks of age were used for experiments unless otherwise indicated.

Banked cryopreserved B16F10 melanoma cells (obtained from ATCC in 2007) were defrosted and cultured in T-75 flask for 48 hours in complete RPMI-1640 medium containing 5% FBS, 1% penicillin and streptomycin antibiotics, and 1 mmol/L L-glutamine. Because banked cells at identical passage were used for all animal studies, their identity was not verified in the last year, but the cells were reverified as negative for known murine viruses and *Mycoplasma* by the Animal Health Diagnostic Laboratory, Frederick National Laboratory. WT or $Cd47^{-/-}$ littermate C57BL/6 mice were subcutaneously injected with PBS-washed B16F10 melanoma cells (1×10^6 cells) into the hind limb. Tumor size was measured every other day using calipers for 15 days. In the CD47 blockade studies, doses (intratumoral, 50 μg/mouse) of anti-CD47 miap301 (eBioscience; cat. #16-0471-85) or isotype rat Ig (eBioscience; cat. #02-9602) were administered on days 7 and 15, and tumor volume was measured every other day until day 21.

Reagents

4,6 diamidino-2-phenylindole (DAPI; cat. #D9542), rat serum (cat. #R9759), and rabbit serum (cat. #R9133) were purchased from Sigma-Aldrich. Aqua live/dead was from Thermo Fisher Scientific (cat. #L3495), UV Zombie was from BioLegend (cat. #423107), and ACK lysis buffer was purchased from Lonza (cat. #10-548E).

NK cell isolation

Total peripheral NK cell populations from mouse spleens were isolated (>90% purity) using an NK Isolation Kit II (MACS, Miltenyi Biotec; cat. #130-115-818) using MACS LS Columns (Miltenyi Biotec; cat. #130-042-401) following the manufacturer's instructions. Isolated NK cells were cultured in complete RPMI without or with IL15 (5–40 ng/mL).

Cytotoxicity assay

Purified NK cells from WT and $Cd47^{-/-}$ mouse spleens were tested for their cytotoxic potential against B16 tumor cells. Freshly isolated NK cells or NK cells cultured with IL15 were incubated with B16 tumor cells with different effector-to-target ratios (E:T; 1:1, 5:1, and 10:1). Cytotoxicity was determined by measuring the fluorescence intensity of the CellTox Green Dye (CellTox Green Cytotoxicity, Promega). Fluorescence intensity correlates with the loss of cell membrane integrity caused by cell death. This assay allows real-time kinetic cytotoxicity measurements because the same well can be measured multiple times, as the fluorescent signal remains constant after 72 hours. B16 cells (5,000 cells/well) were seeded in 96-well black-bottom plates (Greiner). NK cells were added in different E:T ratios to wells containing CellTox Green Dye. Wells without cells were used as a background control. Cell death was determined at 0, 12, 24, and 48 hours of incubation by measuring the fluorescence intensity (485/520 nm excitation/emission) with a TECAN microplate reader. The values obtained from the background control were subtracted from the values obtained from the different experimental conditions.

Apoptosis analysis

Cells were stained with annexin V according to the manufacturer's instructions (BD Biosciences; cat. #550474). Cells were washed in PBS and resuspended in 1 × annexin binding buffer containing allophycocyanin-conjugated annexin V. After 15 minutes of incubation at room temperature, cells were diluted in 1 × annexin V binding buffer and analyzed by flow cytometry.

Mitochondrial stress analysis

Mitochondrial oxygen consumption rate (OCR) and extracellular acidification rate (ECAR) of CD47-sufficient and CD47-deficient NK cells were compared using a Seahorse Bioscience XF^{e}24 analyzer in combination with the Seahorse Bioscience XF Cell Mito Stress Test assay kit (Agilent Technologies; cat. #103015-100). Briefly, NK cells from spleens of WT and $Cd47^{-/-}$ littermate mice were isolated and plated at 0.75×10^6 cells/well in 24-well plates (Seahorse Bioscience) into XF Base Medium (Seahorse Bioscience) with added 10 mmol/L glucose, 1 mmol/L sodium pyruvate, and 2 mmol/L L-glutamine, pH 7.4. Subsequently, analyses of OCR and EACR were performed in a Seahorse analyzer. The OCR and EACR values were obtained during baseline (prior to addition of any Mito Stress Test substances) and after the addition of 0.5 μmol/L oligomycin, 1 μmol/L FCCP, and 0.5 μmol/L rotenone + 0.5 μmol/L antimycin A. Background values only from media were subtracted, and data

were corrected by subtracting nonmitochondrial respiration (measured after the injection of rotenone + antimycin A) from all measured OCR values.

Reactive oxygen species assay

Intracellular reactive oxygen species (ROS) of NK cells were quantified using Fluorometric Intracellular ROS Kit (Sigma-Aldrich) according to the manufacturer's instructions. Briefly, isolated NK cells from WT and littermate *Cd47*$^{-/-}$ mice were subjected to Seahorse Mito Stress analysis with ATP synthase inhibitor oligomycin (0.5 μmol/L), mitochondrial uncoupler carbonyl cyanide 4-(trifluoromethoxy) phenylhydrazone (FCCP; 1 μmol/L), and complex I + II inhibitors rotenone (0.5 μmol/L) + antimycin A (0.5 μmol/L). Cells were then incubated with the ROS detection reagent, and the red fluorescence intensity was measured on a flow cytometer.

RNA extraction, quantitative real-time PCR, and primer sequences

RNA was purified using the RNeasy Microkit (Qiagen) or TRIzol (Ambion, a part of Life Technologies) following the manufacturer's instructions. RNA content was quantified by NanoDrop 8000 (Thermo Fisher Scientific), and 500 ng of RNA was reverse transcribed to cDNA using Thermo Scientific Maxima First-Strand cDNA Synthesis Kit (cat. #K1641). Quantitative real-time PCR was performed with SYBR Green using primers for specific genes (Supplementary Table S1) using at least three replicates per group and analyzed on CFX96 Real-Time System (Bio-Rad). Relative transcript abundance was determined by using the $\Delta\Delta C_t$ or ΔC_t method after normalization with *β-Actin* and *Gapdh*. All samples were run in triplicate. Error bars represent standard error of mean (SEM).

Tumor processing

Tumors were cut into small pieces and enzymatically dissociated with Collagenase/Dispase (Roche; cat. #269638; final concentration 1 mg/mL) and DNase 1 (Sigma; cat. #D4527; final concentration 100 μg/mL). The suspension was centrifuged at 50 × *g* for 5 minutes to separate tissue debris, and supernatant cell suspension was filtered through a 70-μm strainer, followed by centrifugation with 330 × *g* for 5 minutes. Red blood cells (RBC) were lysed using ACK buffer, and cells were suspended in FACS buffer followed by staining or sorting.

Flow cytometry and cell sorting

Single-cell suspensions from organs and tissues were stained with optimized antibody dilutions for 15 minutes at 4°C (Supplementary Table S2). Antibodies were directly conjugated to Brilliant Ultraviolet (BUV)395, Brilliant Violet (BV)786, BV711, BV650, BV605, Pacific Blue (PB), fluorescein isothiocyanate (FITC), phycoerythrin (PE), PE-Cy5.5, PE-Texas Red, peridinin–chlorophyll–protein complex (PerCP)-Cy5.5, PE-Cy7, allophycocyanin (APC), APC-Alexa 700, or biotin. Biotinylated antibodies were revealed with streptavidin APC-eFluor780. Cells were resuspended in FACS buffer (1% BSA + 0.01% NaN_3 in PBS1x, filtered) and incubated with rat plus rabbit serum, followed by incubation with antibody cocktail against surface molecules. For intracellular staining, cells were fixed (IC Fixation Buffer, eBioscience) and permeabilized (Permeabilization Buffer 10×, eBioscience). Dead cells were excluded through DAPI uptake or Aqua live/dead staining. Doublets were excluded through forward scatter–height by forward scatter–width and side scatter–height by side scatter–width parameters. Cells were acquired on an LSRFortessa SORP (BD Biosciences), and data were analyzed using FlowJo (Tree Star). Cell sorting was performed on a FACSAria II (BD Biosciences), and cell purity after sorting was >99%.

RNA sequencing library construction and Illumina sequencing

RNA sequencing (RNA-seq) library preparation and sequencing were performed as described previously (11). Briefly, $Lin^{-}NK1.1^{+}NKp46^{+}$ cells were sorted from spleens of naïve and B16F10 tumor–bearing mice. Total RNA was isolated from sorted cells using TRIzol, and DNase treatment was performed using the RNase-free DNase set (Qiagen). RNA quality was checked using an Agilent 2100 Expert bioanalyzer (Agilent Technologies). RNA samples falling below the threshold of 8.0 (scored from 1–10) were omitted from the study. Ribosomal RNA was removed using biotinylated, target-specific oligos combined with Ribo-Zero rRNA removal beads. The RNA was fragmented and copied into first-strand cDNA, followed by second-strand cDNA synthesis using DNA polymerase I and RNase H. The resulting double-strand cDNA was used as the input to a standard Illumina library prep with end repair, adapter ligation, and PCR amplification being performed. The final purified product was quantitated by qPCR before cluster generation and sequencing. Paired-end sequencing (2 × 150 bp) of stranded total RNA libraries was performed on one HiSeq run with Illumina HiSeq3000/4000 chemistry pair end sequencing. The samples have 99 to 148 million pass filter reads, with a base call quality of above 92% of bases with Q30 and above.

HiSeq Real-Time Analysis software (RTA 1.18) was used for processing image files. Illumina bcl2fastq1.8.4 was used to demultiplex and convert binary base calls and qualities to fastq format. The sequencing reads were trimmed of adapters and low-quality bases using Trimmomatic (version 0.30), and the trimmed reads were mapped to mouse reference genome (GRCm38/mm10) and Gencode annotation M9 using STAR (version 2.5) with two-pass alignment option. RSEM (version 1.2.22) was used for transcript quantification.

RNA-seq data processing and analysis

The reference genome and annotation from GENECODE Mouse (mm10) was used for further downstream analyses. An in-house pipeline (Pipeliner: https://github.com/CCBR/Pipeliner) was used for data analysis. Briefly, to remove the adapter sequences, cutadapt/1.14 was used followed by fastQ Screen v0.9.3 to screen the library for its composition. For quality control, the tool fastqc/0.11.5 was used, and the spliced transcripts alignment to a reference genome and counting the number of reads per gene were performed by STAR/2.5.2b. The mapped reads in the genomic features were counted by subread/1.5.1, and the distribution of these reads was calculated by rseqc/2.6.4 along with the estimation of strandness of the reads. The library complexity was estimated by preseq/2.0.3. To mark duplicate reads and estimate the gene coverage, the program picard/1.119 was used, and for the overall statistics of input data sets, samtools/1.5 was used. For differential expression analysis, the low abundant gene threshold was set to include genes with ≥0.5 counts per million in at least ≥ 4 samples. In order to generate the gene lists based on different contrast, the R Bioconductor package DESeq2 was used. Principal component analysis (PCA) was performed using Partek

Genomics Suite (v 6.5), and gene set enrichment analysis (GSEA) was performed using software provided by the Broad Institute. RNA-seq data are deposited on the NCBI Sequence Read Archive (GSE113876).

Statistical analysis

Statistical analysis of groups with limited variance was performed using GraphPad Prism 7 (Version 7.01). Comparison between two groups was done via two-sided Student *t* test. Differences with a *P* value less than 0.05 were considered statistically significant. Error bars indicate SEM unless otherwise indicated. cBioPortal tools were used to calculate *P* values for TCGA data.

Results

CD47 mRNA expression is positively correlated with melanoma overall survival

Consistent with the hypothesis that CD47 protects tumor cells from innate immune surveillance, elevated expression of CD47 in some solid tumors and hematologic malignancies is correlated with a poorer prognosis (24–26). However, analysis of CD47 mRNA expression data in TCGA revealed the opposite for a set of 469 melanomas with RNA-seq data, including 461 with survival data (Fig. 1A). Segregating the melanoma RNA-seq data with a mean cutoff showed that patients with melanoma with tumor CD47 mRNA expression above the mean had significantly longer overall survival than those with expression below the mean (111 months and 62.7 months median survival, respectively, log-rank test $P = 0.0017$). The 65 patients with CD47 expression >1 SD above the mean showed no further improvement (median survival of 103.2 months, log-rank test $P = 0.14$). However, the 85 cases with CD47 mRNA expression more than 1 SD below the mean had a shorter median overall survival of 44.5 months ($P = 6.8 \times 10^{-6}$ compared with the remaining 374 tumors). Disease-free survival was also significantly shorter in the cases with the lowest CD47 expression (36 months vs. 56 months, log-rank test $P = 0.002$; Supplementary Fig. S1A). Thus, increased *CD47* gene expression in human melanomas is dose dependently associated with improved survival.

Because these data were inconsistent with the prevailing "don't eat me" hypothesis, a prediction that tumors with elevated CD47 have poorer survival because they are resistant to phagocytosis by macrophages, we examined coexpressed genes in the TCGA data to identify potential immune mechanisms through which increased intratumoral CD47 mRNA expression could improve melanoma survival. Among the relevant gene sets examined, we identified the highest significance for NK cell–related genes (Fig. 1B). Because significant correlations between expression of these genes and CD47 were generally lacking in other cancers (Supplementary Fig. S1B), this association appears to be specific for melanoma. Using reported gene signatures for naïve versus activated NK cells (27), the highest correlations were observed for an early NK effector signature, and greater than mean expression of one or more of these signature genes was strongly correlated with increased overall survival (148 months vs. 48 months; Fig. 1C, $P = 6.9 \times 10^{-9}$). Lack of correlation with overall survival in other cancers indicated that the relationship between NK early activation gene expression and outcome is also specific for melanomas (Supplementary Fig. S1C).

A strong positive correlation between CD47 and IL15 mRNA expression in human melanomas suggested that increased expression of this cytokine could contribute to activation of NK cells in melanomas that express elevated CD47 (Fig. 1D). Consistent with this hypothesis, IL15 mRNA expression greater than the mean was associated with improved overall survival ($P = 1.5 \times 10^{-8}$) and disease/progression-free survival for the patients with melanoma ($P = 2.3 \times 10^{-3}$; Supplementary Fig. S1D and S1E).

Thrombospondin-1 is a CD47-dependent inhibitor for NK cells

CD47 is an inhibitory receptor for thrombospondin-1 on vascular cells and T cells (28–31). Interaction between CD47 and thrombospondin-1 inhibits T-cell receptor (TCR) signaling in T cells and VEGF-stimulated endothelial cell proliferation (9, 30, 32). Similarly, a 2 nmol/L concentration of thrombospondin-1, which is sufficient to engage CD47, but not other known thrombospondin-1 receptors, significantly reduced proliferation of isolated murine NK cells as assayed by Ki-67 staining (Fig. 2A). Further, thrombospondin-1 treatment of WT NK cells, but not $Cd47^{-/-}$ NK cells, inhibited basal and IL15-stimulated proliferation as assessed using an MTS assay (Fig. 2B; Supplementary Fig. S2A). Both mRNA and protein expression of CD69 and protein expression of CD11b and CD11c, which are induced upon NK activation (27), were similarly downregulated in LPS-activated NK cells treated with thrombospondin-1 (Fig. 2C and D; Supplementary Fig. S2B and S2C).

We confirmed the inhibitory activity of thrombospondin-1 using human NK cells. NK-92 cells cultured with IL2 showed significantly inhibited proliferation in the presence of thrombospondin-1. Such inhibition was reversed when CD47 was blocked using the CD47 antibody B6H12, which similarly stops inhibitory thrombospondin-1 signaling in T cells (ref. 33; Fig. 2E). Therefore, the inhibitory activity of thrombospondin-1 requires CD47 in murine and human NK cells.

Anti-CD47 enhanced intratumor NK cell activity

The CD47 antibody miap301 similarly blocks inhibitory thrombospondin-1 signaling in murine T cells and enhances syngeneic tumor cell killing by murine CD8 T cells (29, 34). Correspondingly, treating murine NK cells with miap301 for 48 hours in culture enhanced cell-surface CD69 expression and intracellular IFNγ. However, intracellular granzyme B (GzmB) was unchanged (Fig. 3A). The response of anti-CD47 treatment was comparable to anti-NK1.1, but not to IL15, treatment in terms of CD69 expression, GzmB, and IFNγ (Fig. 3A). Lack of these responses in $Cd47^{-/-}$ NK cells confirmed specificity (Fig. 3B).

Extending the *in vitro* enhancement of NK cell function by miap301 to study NK cell immunity in a mouse tumor model is complicated by the dual function of this antibody to block both thrombospondin-1 and SIRPα binding. The anti-human CD47 B6H12 is efficacious in multiple xenograft tumor models, which is attributed to enhancing SIRPα-dependent phagocytic clearance by macrophages, but miap301 generally does not inhibit growth of syngeneic tumors in immune-competent mice (25). Therefore, we tested the effect of miap301 on NK cell function in the syngeneic B16 model. Intratumoral anti-CD47 treatment with miap301 slowed the growth of B16 tumors compared with tumors in mice treated with isotype-matched rat Ig (Fig. 3C). Treatment of tumor-infiltrating NK cells isolated from B16 tumors treated with miap301 but not the control antibody significantly increased intracellular IFNγ after 48 hours of treatment (Fig. 3D–F). Such *in vitro* treatment increased intracellular IFNγ and GzmB

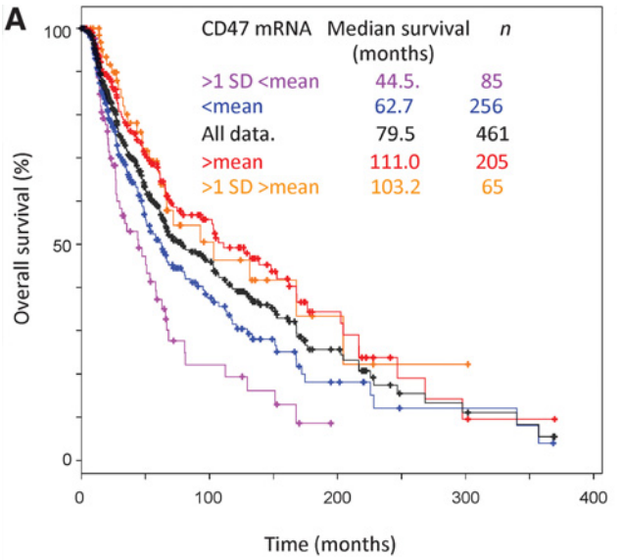

B

Gene	Spearman correlation	P	NK cell gene function
IFIH1	0.597	6.2e–47	Early NK effector
TBX21 (TBET)	0.326	3.5e–13	Early NK effector
STAT1	0.507	4.0e–32	Early NK effector
IFNG	0.437	2.2e–23	Early NK effector
GBP4	0.431	8.0e–23	Early NK effector
IL2RA (CD25)	0.410	1.5e–20	Early NK effector
KLRG1	0.324	5.3e–13	Late NK effector
NLRC5	0.393	7.0e–19	NK sustained effector
GZMA	0.388	1.9e–18	Naïve NK signature
GZMB	0.316	2.1e–12	Naïve NK signature
GZMK	0.380	1.2e–17	NK effector
NCR1 (NKp46)	0.247	5.3e–8	Naïve NK signature
KLRB1 (NK1.1)	0.320	1.2e–12	Naïve NK signature
KLRC1	0.397	2.6e–19	NK receptor
KLRK1 (NKG2D)	0.367	1.7e–16	NK receptor
KLRD1 (CD94)	0.393	2.9e–19	NK receptor

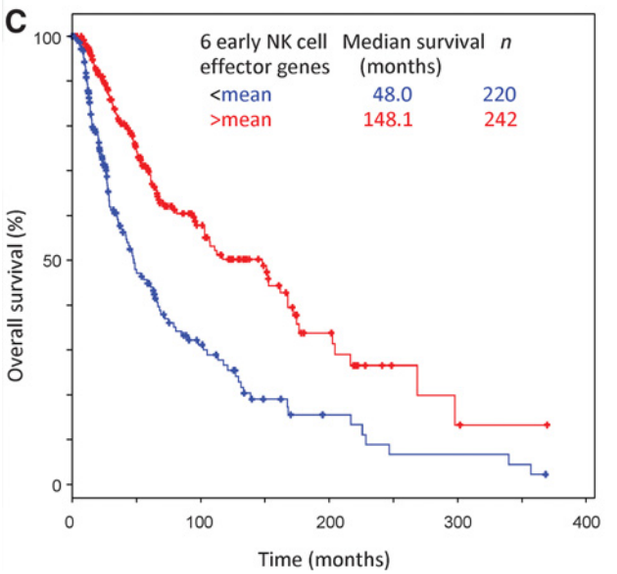

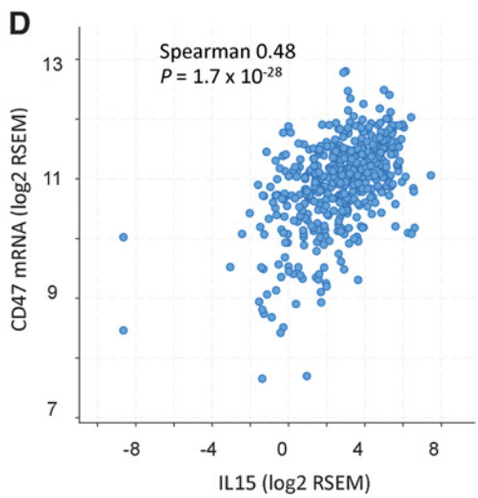

Figure 1.

Improved survival of patients with melanoma with elevated CD47 expression is associated with markers of early effector NK cells. **A,** Dose-dependent correlation between CD47 mRNA expression and overall survival in TCGA melanoma data. **B,** Analysis of TCGA RNA-seq data for coexpression correlations between CD47 mRNA and naïve or activated NK signature genes as defined in ref. 27. Spearman correlation and *P* values determined using cBioPortal tools are presented for TCGA RNA-seq data from 469 patients with cutaneous melanoma. **C,** Overall survival of patients with mRNA expression of the six early NK effector signature genes greater than (red) or less than the mean (blue) aggregate values determined by RNA-seq analysis ($n = 462$ patients). **D,** IL15 expression correlates with mRNA expression in TCGA melanoma data ($n = 469$ patients).

levels in B16-infiltrating NK cells, but not in infiltrating CD8 T cells (Fig. 3G–I). Therefore, our previously reported increase in intratumoral GzmB expression following CD47 knockdown in several syngenic tumor models may be produced primarily by NK cells (6).

Expression of CD47 on NK cells limits their proliferation and effector state

IL15 dose dependently increased the frequency of NK1.1$^+$ cells in cultured WT and *Cd47*$^{-/-}$ splenocytes, but the response to IL15 was greater in *Cd47*$^{-/-}$ (Fig. 4A). Similarly, cell activation and

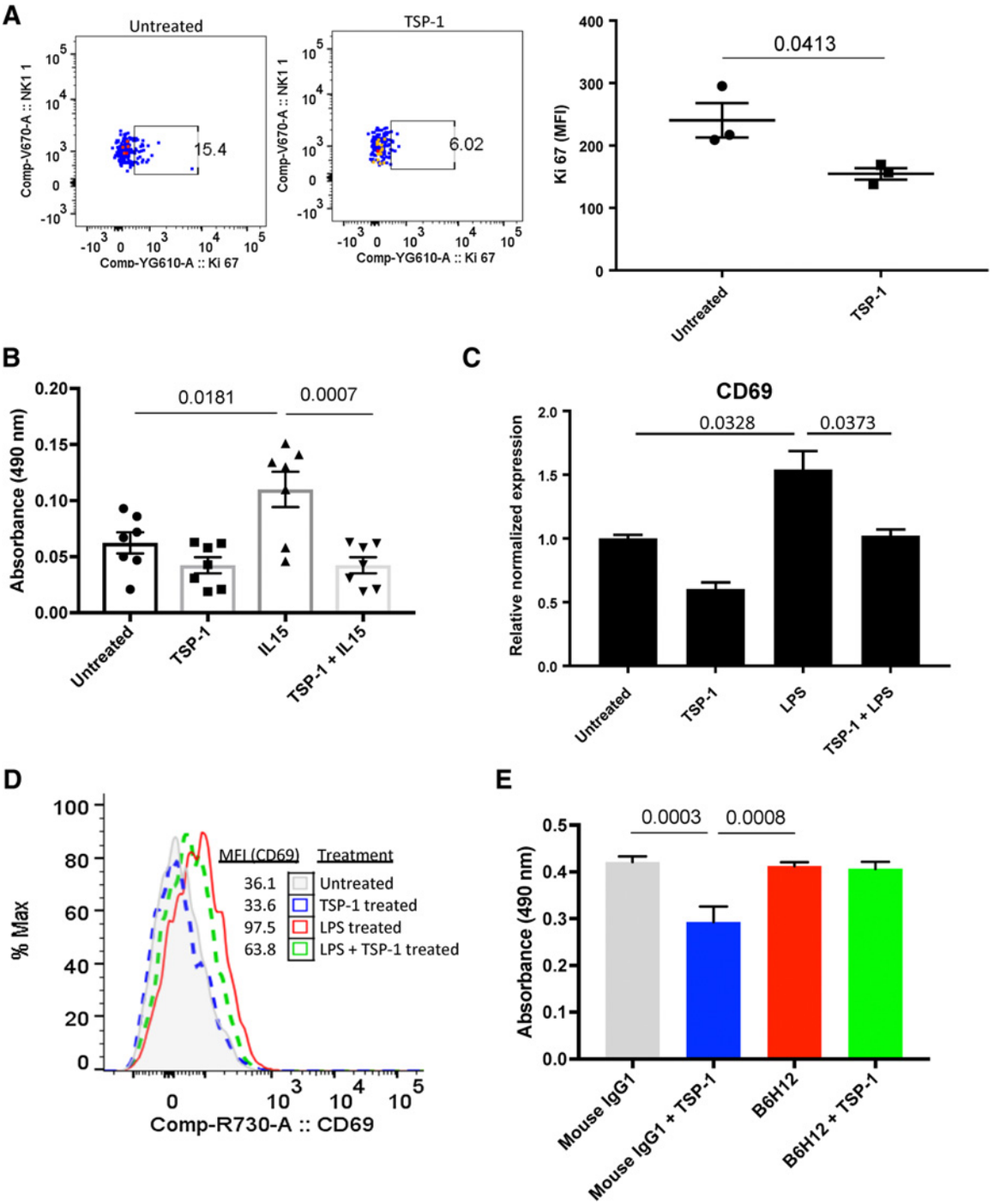

Figure 2.

Thrombospondin-1 inhibits NK cell proliferation and activation. NK cells were isolated from spleens of WT mice by a MACS NK isolation kit. **A,** Cells were cultured in serum-free RPMI for 24 hours with/without thrombospondin-1 (2 nmol/L), followed by fixation, permeabilization, and intracellular staining for Ki-67; $n = 3$ biological replicates; error bars, SEM. **B,** NK cells were cultured in serum-free RPMI with/without IL15 (10 ng/mL), and MTS absorbance was measured after 24 hours of culture in the presence or absence of thrombospondin-1 (2 nmol/L); $n = 7$ biological replicates; error bars, SEM. **C,** Isolated NK cells were divided into four groups and cultured in serum-free RPMI with thrombospondin-1 (2 nmol/L), LPS (1 μg/mL), or both. mRNA abundance (relative to *β-Actin*) and (**D**) cell-surface protein levels of CD69 were measured by RT-qPCR (LPS vs. TSP-1 + LPS treatments, $P = 0.0373$; $n = 3$ biological replicates; error bars, SEM) and flow cytometry (representative), respectively. **E,** Human NK-92 cells were cultured in serum-free RPMI with 100 IU IL2 and treated either with mouse IgG (1 μg/mL) or B6H12 (1 μg/mL) in the presence or absence of human thrombospondin-1 (2 nmol/L), and MTS absorbance was measured after 48 hours; $n = 5$ technical replicates; error bars, SEM. MFI, mean fluorescence intensity.

A

Treatment	IL2 (MFI)	CD69 (MFI)	GzmB (MFI)	IFNγ (MFI)	CD122 (MFI)
Untreated	386	60.7	221	308	66.8
Anti-NK1.1	351	74.6	276	615	48.4
Anti-CD47	370	75.6	273	572	49.9
IL15	295	106	496	392	45.5

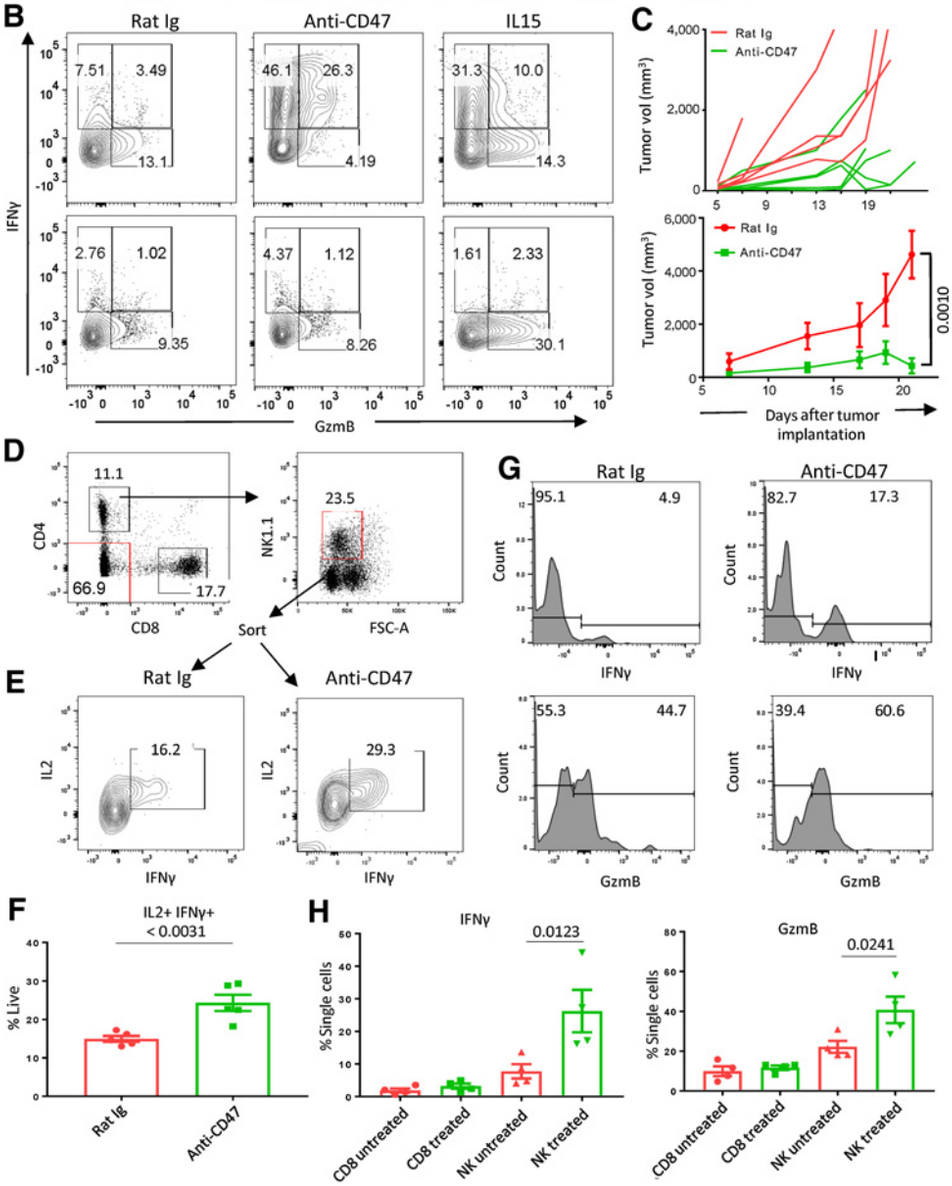

Figure 3.

Miap301 treatment enhances effector protein expression in NK cells and reduces tumor growth. **A,** NK cells were isolated from WT spleens and treated with anti-CD47 (miap301, 5 μg/mL), anti-NK1.1 (5 μg/mL), or IL15 (40 ng/mL) for 48 hours with GolgiStop during the last 4 hours in culture; $n = 3$ biological replicates. The table shows the mean fluorescence intensity (MFI) of IL2, CD69, GzmB, IFNγ, and CD122 proteins within different treatment groups. **B,** Plots show intracellular expression of GzmB and IFNγ in isotype rat Ig, anti-CD47, and IL15-treated WT (top) and *Cd47*$^{-/-}$ NK cells (bottom). **C,** B16F10 tumors were implanted in the hind limb of C57BL/6 mice, and two doses of rat Ig or anti-CD47 Ab (intratumoral, 50 μg/mouse) were administered on days 7 and 15. Tumor volume (vol) was measured every other day. WT versus *Cd47*$^{-/-}$ mice; $P = 0.001$; $n = 5$ biological replicates; error bars, SEM. **D** and **E,** Animals were sacrificed on day 21, tumors were incised, and DAPI^{-}CD45.2^{+}CD4^{-}CD8^{-}CD3^{-}NK1.1^{+} cells were sorted from single-cell suspension and treated with rat Ig (5 μg/mL) or anti-CD47 (5 μg/mL) for 48 hours with GolgiStop during the last 4 hours in culture. Cells were intracellularly stained for IL2 and IFNγ; $n = 5$. **F–I,** Representative plots and frequencies of intracellular IFNγ and GzmB expression in rat Ig or anti-CD47–treated tumor-infiltrating CD8 T and NK cells; $n = 4$–5 biological replicates; error bars, SEM.

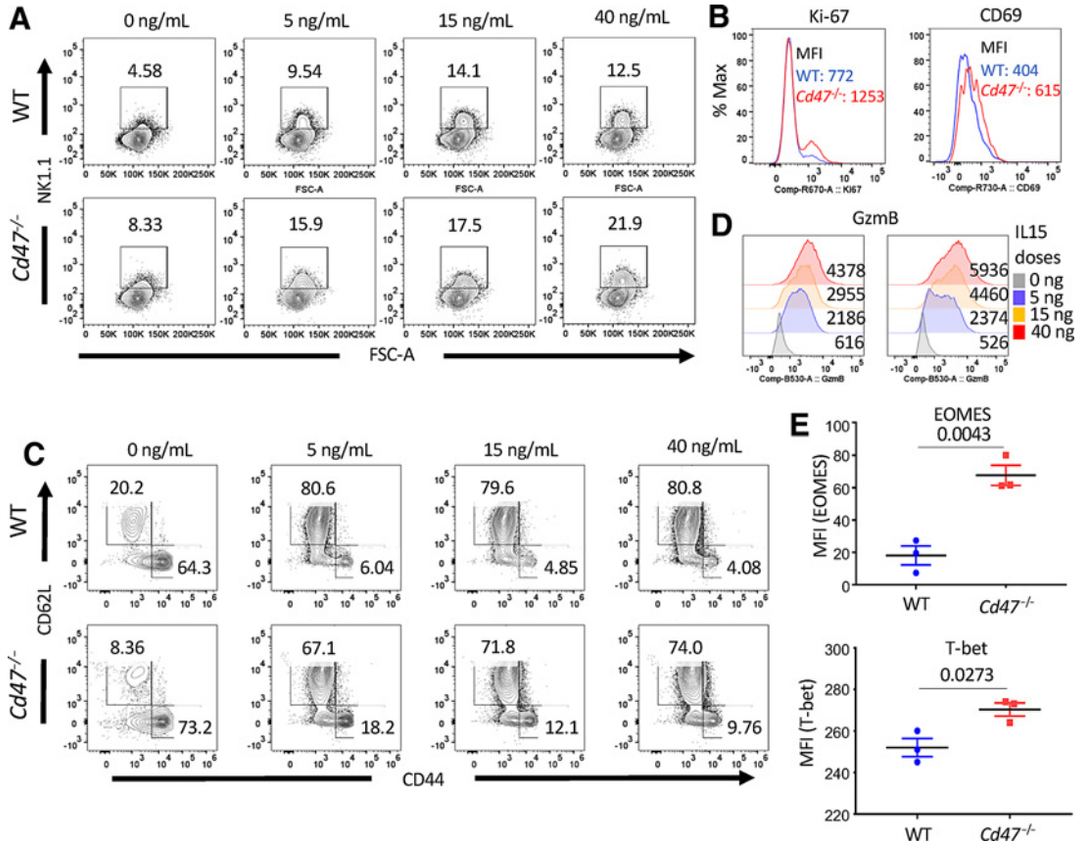

Figure 4.

CD47 limits some effector properties of NK cells. **A,** Single-cell suspensions from a pool of 3 WT and 3 *Cd47*$^{-/-}$ littermate mouse spleens were treated with IL15 (5, 15, and 40 ng/mL) for 24 hours in complete RPMI (10% FCS). Cells were FcR blocked and stained for Aqua live/dead, NK1.1, and CD69, followed by intracellular staining for Ki-67. Frequencies of NK1.1^{+} cells within the cultured splenocytes were detected by flow cytometry. Data are representative of two independent experiments. **B,** Histograms show expression of Ki-67 and CD69 within the NK1.1^{+} population of the IL15 (5 ng/mL)-treated group. Values on the plots are MFI of indicated protein in NK1.1^{+} cells. Data are representative of two independent experiments. **C,** NK cells were enriched from pooled splenocytes of WT and *Cd47*$^{-/-}$ littermate mice and cultured with IL15 (5, 15, and 40 ng/mL) for 24 hours and stained for CD44 and CD62L. Data are representative of two independent experiments. **D,** Histograms show expression of GzmB within the NK1.1^{+} population; values indicate MFI in NK1.1^{+} cells. Data are representative of two independent experiments. **E,** NK cells from the spleens of WT and *Cd47*$^{-/-}$ littermate mice were treated with IL15 (5 ng/mL for 24 hours) and stained for intracellular Eomes ($P = 0.0043$) and T-bet ($P = 0.0273$) proteins; $n = 3$ biological replicates; error bars, SEM. MFI, mean fluorescence intensity.

proliferation, assessed by CD69 and Ki-67 staining, respectively, was enhanced in *Cd47*$^{-/-}$ NK1.1^{+} cells (Fig. 4B). Intracellular GzmB staining of splenic NK cells from naïve *Cd47*$^{-/-}$ mice tended to be higher in frequency and count but did not achieve significance (Supplementary Fig. S3A). The mean fluorescence intensity (MFI) of IFNγ and GzmB were comparable between WT and *Cd47*$^{-/-}$ total splenocytes and NK1.1^{+} populations within the total splenocytes cultured with increasing dosages of IL15 (Supplementary Fig. S3B and S3C). NK cells isolated from the spleens of WT and *Cd47*$^{-/-}$ mice cultured with IL15 for 24 hours exhibited downregulated CD44 and upregulated CD62L surface expression (Fig. 4C; Supplementary Fig. S3D). However, *Cd47*$^{-/-}$ NK cells were more CD44 positive and less CD62L positive compared with the WT NK cells (Fig. 4C). An increasing trend of GzmB, T-bet, KLRG1, and TNFα was evident in IL15 treated *Cd47*$^{-/-}$ NK cells relative to similarly treated WT NK cells (Fig. 4D; Supplementary Fig. S3E). IL15 treatment significantly upregulated Eomes and T-bet expression in *Cd47*$^{-/-}$ NK cells relative to that in WT NK cells (Fig. 4E). However, *in vitro* cytotoxic activities of WT and *Cd47*$^{-/-}$ NK cells, both with and without IL15 treatment, were comparable when cocultured with target B16 melanoma cells (Supplementary Fig. S3F).

After continuous culture with IL15 for 72 hours, a decreasing trend of IFNγ and GzmB protein labels was evident in *Cd47*$^{-/-}$ total splenocytes relative to WT counterparts (Supplementary Fig. S4A). Analysis of similarly cultured *Cd47*$^{+/-}$ NK cells revealed that the decrease of *Ifng* and *Gzmb* transcripts was CD47 dose dependent (Supplementary Fig. S4B).

Global transcriptome analysis of WT and *Cd47*$^{-/-}$ NK cells from spleens of naïve mice identified 2,585 genes to be significantly upregulated ($P < 0.05$) in naïve *Cd47*$^{-/-}$ versus WT NK cells, including the effector genes *Ifna2* (IFNα2), *Ifna4* (IFNα4), *Ifna13* (IFNα13), *Gzmc* (granzyme C), *Il2ra* (CD25), *Mapk13* (MAPK13), and *Jun* (c-Jun; Supplementary Fig. S5A; Supplementary Table S3). As expected, *Cd47* was significantly decreased in *Cd47*$^{-/-}$ NK cells (Supplementary Fig. S5A; Supplementary Table S3). An unsupervised GSEA showed upregulation of early effector, sustained effector, interferon, and proliferation gene

signatures, whereas naïve and memory gene signatures were downregulated in naïve *Cd47*$^{-/-}$ NK cells compared with WT counterparts (Supplementary Fig. S5B; Supplementary Table S4).

Pathway analysis showed altered responses of NK cells in the absence of *Cd47*. An upregulation of immune-related pathways, including immune response (G:0002376, GO:0002682, GO:0050776, R-HAS-168249, and GO:0006955), cytokine production, and signal transduction (go:0007165; Supplementary Fig. S5C), as well as significant downregulation of NK-mediated cytotoxicity and MAPK, EGFR, and DAP12 signaling pathways were evident in *Cd47*$^{-/-}$ NK cells (Supplementary Fig. S5C). Cytoscape functional and molecular interaction networks in NK cells revealed that the immune- and inflammation-related genes were significantly altered upon *Cd47* depletion (Supplementary Fig. S5D).

CD47 limits mitochondrial metabolism and ROS production in NK cells

CD47 controls mitochondrial homeostasis and metabolism and, in T cells, apoptosis pathways involving the mitochondrial regulators Drp1 and BNIP3 (32, 35–37). Mitochondrial electron transport can generate ROS that control intrinsic apoptosis pathways (38). Global gene-expression analysis demonstrated that the top upregulated pathways in *Cd47*$^{-/-}$ NK cells include metabolic regulation and ion transport, whereas the top downregulated pathways include mitochondrial protein regulation and mitochondrial organization (Supplementary Fig. S5C). To investigate whether CD47 regulates mitochondrial and glycolytic metabolism in NK cells, we measured the mitochondrial OCR and ECAR in NK cells subjected to mitochondrial stress. Sequentially blocking key enzymes of the respiratory chain of mitochondria using oligomycin, FCCP, and a mix of rotenone and antimycin A was performed to measure ATP production, maximum respiration, and nonmitochondrial respiration, respectively. Basal mitochondrial flux assessed by OCR values was similar for WT and *Cd47*$^{-/-}$ NK cells. In contrast, basal glycolytic flux assessed by ECAR values was higher in *Cd47*$^{-/-}$ NK cells (Fig. 5A and B). The ATP turnover values in WT and *Cd47*$^{-/-}$ NK cells were comparable (56.6 ± 19.4 vs. 67.2 ± 0.3). However, the proton leak values in *Cd47*$^{-/-}$ NK cells (38.7 ± 13.5) were higher than in WT NK cells (14.5 ± 0.5). In addition, the spare respiratory capacity in *Cd47*$^{-/-}$ NK cells (191.9 ± 20.7) was higher than that in WT NK cells (151.1 ± 9.2). Therefore, WT and *Cd47*$^{-/-}$ NK cells differ in glucose metabolism and respond differently to inhibition or uncoupling of mitochondrial respiratory pathways.

We measured ROS in WT and *Cd47*$^{-/-}$ NK cells after 1 and 24 hours of cell culture with oligomycin, FCCP, rotenone, and antimycin A. The frequency of intracellular ROS-positive *Cd47*$^{-/-}$ NK cells was higher than in WT NK cells subjected to 1 hour of mitochondrial stress (Fig. 5C). Incubation for 24 hours with the mitochondrial stressors upregulated intracellular ROS accumulation both in WT and *Cd47*$^{-/-}$ NK cells, with a significantly higher mean intracellular ROS intensity in *Cd47*$^{-/-}$ NK cells than in WT NK cells (Fig. 5C).

CD47-deficient NK cells undergo apoptosis upon stimulation or under stress

The higher metabolic activity and mitochondrial stress responses of CD47-deficient NK cells results in accumulation of more intracellular ROS, suggesting that CD47 deficiency may increase NK cell apoptosis. Annexin V staining of untreated NK cells from WT and *Cd47*$^{-/-}$ mice was comparable. However, mitochondrial stress induced by treating NK cells with oligomycin, FCCP, rotenone plus antimycin A for 24 hours resulted in higher annexin V–positive staining of *Cd47*$^{-/-}$ NK cells (Fig. 5D–F).

CD47 deficiency in the tumor microenvironment augments B16 melanoma growth

We previously reported that combining antisense CD47 morpholino knockdown and local tumor irradiation or local irradiation of B16 tumors in *Cd47*$^{-/-}$ mice significantly delays the growth of B16 melanoma relative to irradiation alone in immune-competent C57BL/6 mice (6, 39). However, CD47 knockdown in the absence of irradiation only minimally affected B16 tumor growth (6, 39). Implanted B16 tumors grew faster in *Cd47*$^{-/-}$ than in WT mice (Fig. 6A–C).

B16 cells elicit a weak cytotoxic T-cell response due to downregulated MHC class I expression (40), suggesting that the reported CD8 T cell–dependent tumor ablation could also involve NK cells. Frequencies of NK1.1^{+} and NKp46^{+} NK cells significantly dropped within the spleens of *Cd47*$^{-/-}$ mice on day 15 after B16 melanoma implantation (Fig. 6D–G). Flow-cytometric analysis of the NK1.1^{+} compartment in spleens showed a significant increase of CD44 and decrease of CD62L levels in *Cd47*$^{-/-}$ NK cells compared with WT counterparts (Fig. 6H and I). Reduction of the CD62L level in *Cd47*$^{-/-}$ NK cells following *in vitro* stimulation (Fig. 4C) as well as in tumor-bearing mice indicates reduced functionality of *Cd47*$^{-/-}$ NK cells. Concomitantly, increased expression of the exhaustion marker TIGIT and the ATPase CD39 within the CD62L^{+} population of CD47-deficient NK cells further indicated an exhausted and apoptotic phenotype (Fig. 6J and K). Eomesodermin (Eomes) is the master transcriptional regulator of NK cell development, maturation, and function (41) and is downregulated in exhausted NK cells in leukemic mice (42). Similarly, splenic NK cells from *Cd47*$^{-/-}$ tumor–bearing mice exhibited a decreasing trend of Eomes (Fig. 6L). CD127 expression on NK cells correlates with lower GzmB level and a defect in activation (43), and the CD127 level was significantly increased in CD47-deficient NK cells of tumor-bearing mice (Fig. 6M). KLGR1 expression differentiates effector and memory NK cells (44). However, KLRG1 expression did not differ between B16-bearing WT and *Cd47*$^{-/-}$ mice at day 15 (Fig. 6N). Tumor-experienced NK cells express significantly higher levels of PD-1 and PD-L1, suggesting NK exhaustion as well as inhibitory immune regulation (45, 46). Upregulation of PD-1 was also associated with decreased degranulation and impaired cytokine production (45, 47). Consistent with these studies, *Cd47*$^{-/-}$ NK cells expressed significantly higher levels of PD-1 and PD-L1 and significantly less intracellular GzmB compared with WT NK cells (Fig. 6O–Q).

CD47 in the tumor microenvironment controls transcriptional reprogramming of NK cells

We performed global transcriptome analysis of intratumoral and splenic NK cells at day 15 after implantation of B16 melanoma in WT and *Cd47*$^{-/-}$ mice. Intratumoral NK cells from WT and *Cd47*$^{-/-}$ mice showed a low RNA integrity value (Supplementary Fig. S6A) and high divergence by PCA, which precluded further analysis. Therefore, we focused on systemic changes in splenic NK cells. Delineation of population relationships with the

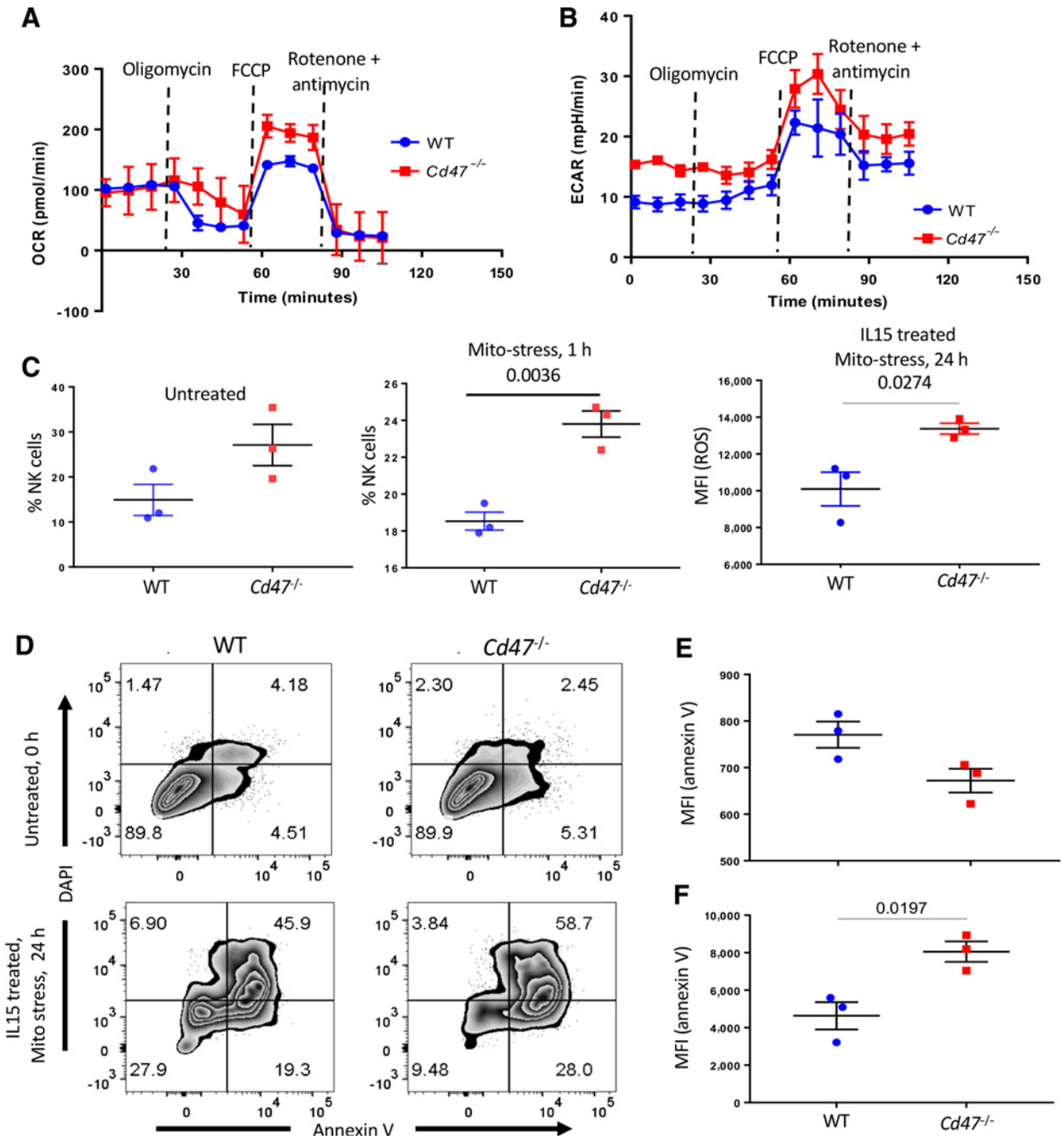

Figure 5.

CD47 limits mitochrondrial metabolism, intracellular ROS accumulation, and apoptosis of NK cells. NK cells were isolated from pooled spleens of WT and *Cd47*$^{-/-}$ mice and subjected to mitochondrial stress by sequential injection of oligomycin, FCCP, and a mix of rotenone and antimycin A; n = pool of 3 biological replicates; error bars, SEM. min, minutes. OCR (**A**) and ECAR (**B**) measured at different time points. **C,** Intracellular ROS accumulation was measured in WT and *Cd47*$^{-/-}$ untreated, 1-hour Mito Stress–treated, and 24-hour Mito Stress–treated NK cells; n = 3 biological replicates; error bars, SEM. **D,** Annexin V staining of WT and *Cd47*$^{-/-}$ NK cells, untreated or treated with mitochondrial stress. **E** and **F,** MFI of annexin V staining in untreated and mitochondrial stress–treated NK cells from spleens of WT and *Cd47*$^{-/-}$ mice; n = 3 biological replicates; error bars, SEM. h, hours.

three most informative principal components showed segregation of the population into four discrete clusters (Fig. 7A). Comprehensive pairwise comparison of NK cells showed upregulation of around 3,000 genes in WT tumor–bearing compared with WT-naïve mice. However, many fewer genes were upregulated in *Cd47*$^{-/-}$ NK cells (total number = 705) than in WT NK cells (total number = 3,012) from tumor-bearing mice (Fig. 7B; Supplementary Table S3). Differential upregulation of inhibitory genes, including *Cish* (CIS), *Mmp9* (MMP-9), *Lag3* (CD223), *Havcr2* (Tim-3), *Tigit* (TIGIT), and *Pdcd1* (PD-1), and

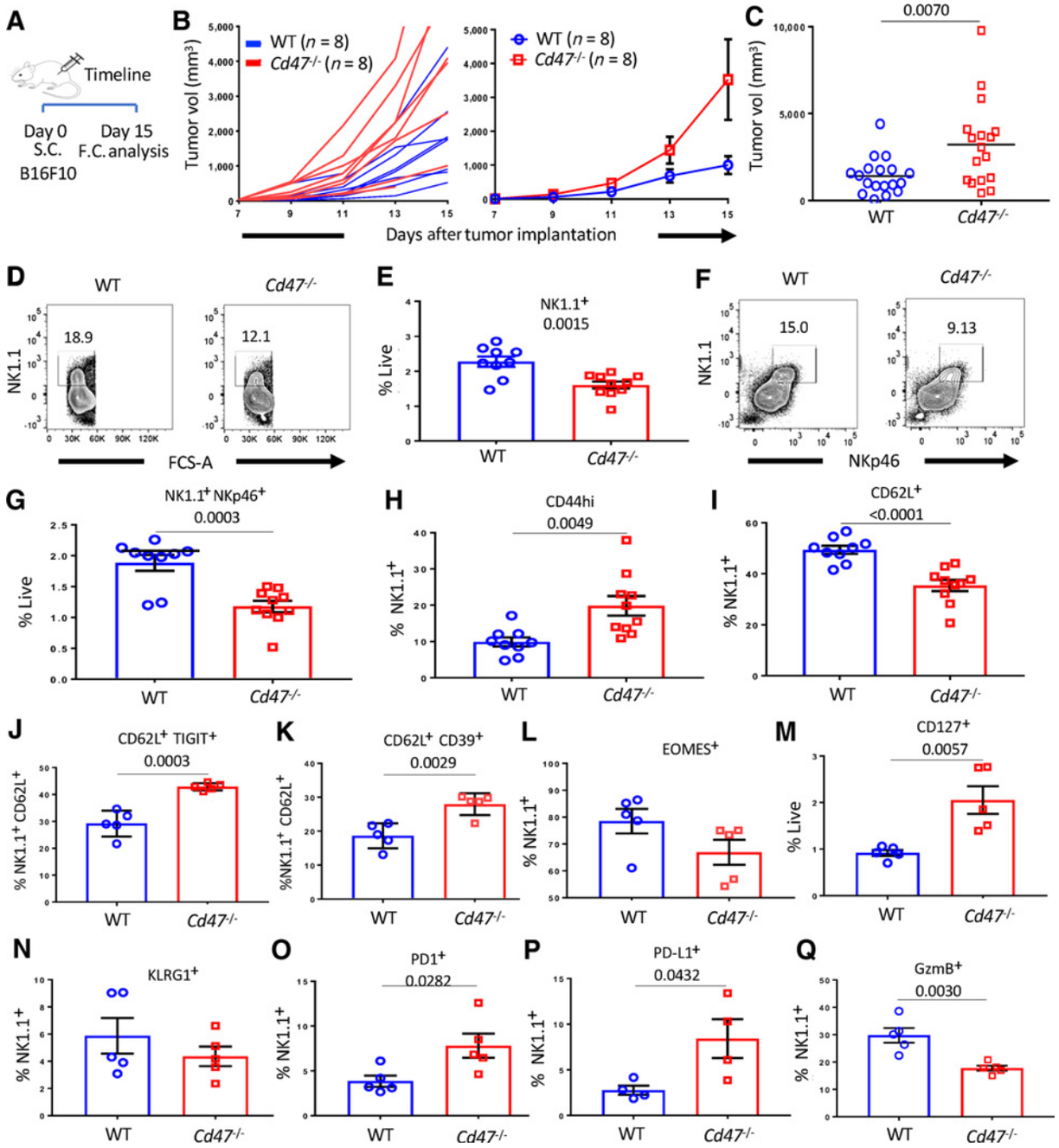

Figure 6.

CD47 limits the growth of B16F10 melanoma in mice. **A,** Timeline of B16F10 tumor implantation and analysis of mice. B16F10 tumors were implanted in the hind limb of C57BL/6 WT and *Cd47*$^{-/-}$ littermate mice (1×10^6 cells/mouse). On day 15 after tumor implantation, mice were euthanized, and single-cell suspensions of spleens were stained with Lin-cocktail (anti-CD4, -CD8, -TCRβ, -B220, -CD19, -Gr1, and -Ter119), anti-NK1.1, and anti-NKp46 in FACS buffer containing Aqua live/dead. Cells were then fixed, permeabilized, and intracellularly stained for the indicated proteins. **B,** Tumor volume was measured every other day for 2 weeks. $n = 8$ biological replicates; error bars, SEM. **C,** Tumor volume was measured on day 15 after tumor implantation (WT vs. *Cd47*$^{-/-}$ mice, $P = 0.007$, $n = 17$–18 mice per group). **D–G,** Representative plots and frequency of live Lin$^-$NK1.1$^+$ cells (WT vs. *Cd47*$^{-/-}$ mice, $P = 0.0015$) and Lin$^-$NK1.1$^+$NKp46$^+$ cells (WT vs. *Cd47*$^{-/-}$ mice, $P = 0.0003$) at day 15 after tumor implantation are shown within the spleens of the mice. $n = 9$–10 mice per group. **H** and **I** and **L–Q,** Frequency of CD44 (WT vs. *Cd47*$^{-/-}$ mice, $P = 0.0049$), CD62L (WT vs. *Cd47*$^{-/-}$ mice, $P < 0.0001$), Eomes, CD127 (WT vs. *Cd47*$^{-/-}$ mice, $P = 0.0057$), KLRG1, PD-1 (WT vs. *Cd47*$^{-/-}$ mice, $P = 0.0282$), PD-L1 (WT vs. *Cd47*$^{-/-}$ mice, $P = 0.0432$), and GzmB (WT vs. *Cd47*$^{-/-}$ mice, $P = 0.003$)–positive NK cells within the spleens of tumor-bearing mice. $n = 4$–5 mice per group; error bars, SEM. **J** and **K,** Frequency of TIGIT (WT vs. *Cd47*$^{-/-}$ mice, $P = 0.0003$) and CD39 (WT vs. *Cd47*$^{-/-}$ mice, $P = 0.0029$)-positive population within CD62L-positive compartment of NK cells. $n = 4$–5 mice per group; error bars, SEM. All data are representative of two independent experiments. vol, volume.

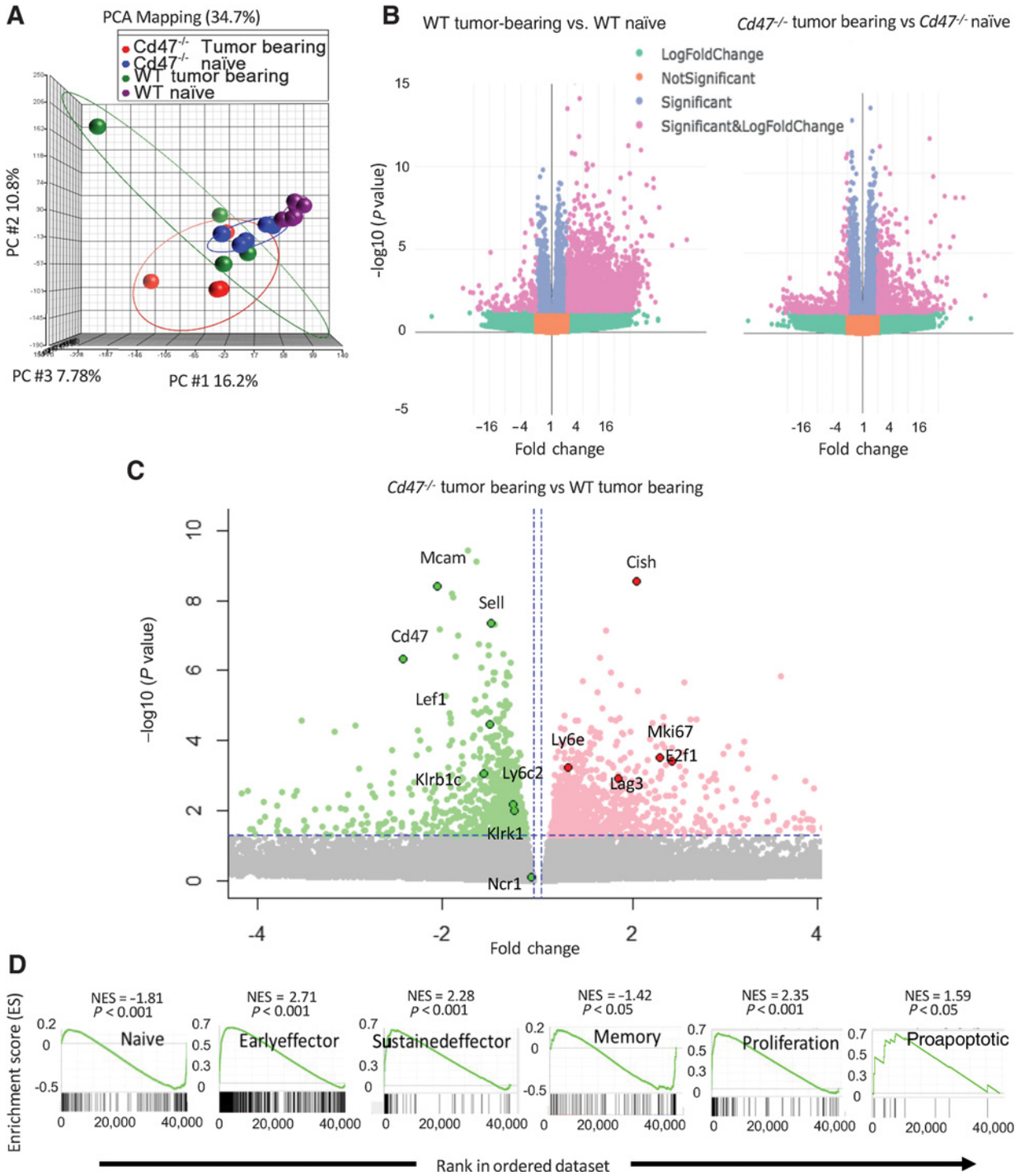

Figure 7.

Transcriptional profile of splenic CD47-deficient NK cells varies from CD47-sufficient NK cells in a murine melanoma model. **A,** PCA on global transcriptome data shows four distinct clusters of naïve WT, naïve *Cd47*$^{-/-}$, B16 tumor–bearing WT, and B16 tumor–bearing *Cd47*$^{-/-}$ NK cells. **B,** Volcano plots show the number of genes upregulated in NK cells of B16-bearing mice compared with their naïve counterparts. **C,** Volcano plot displaying fold change of genes in NK cells of *Cd47*$^{-/-}$ mice relative to WT mice bearing B16 tumor. **D,** GSEA plots in *Cd47*$^{-/-}$compared with WT NK cells of B16-bearing mice.

downregulation of activation genes, including *Sell* (CD62L), *Mcam* (CD146), *Klrk1* (NKG2D), and *Klrc2* (NKG2C), were evident in NK cells from tumor-bearing *Cd47*$^{-/-}$ mice relative to WT counterparts (Fig. 7C; Supplementary Fig. S6B–S6D).

As observed in NK cells from naïve mice (11), significant negative enrichments of naïve and memory NK cell signatures were evident in *Cd47*$^{-/-}$ NK cells from tumor-bearing mice, but sustained effector and proliferation gene signatures were positively enriched in *Cd47*$^{-/-}$ NK cells from tumor-bearing mice (Fig. 7D; Supplementary Table S4). Consistent with our earlier observation (Fig. 5D–F), a proapoptotic gene signature (Qiagen GeneGlobe: Apoptosis and Cell Death, species = mouse) was also upregulated in splenic NK cells from tumor-bearing *Cd47*$^{-/-}$ mice (Fig. 7D). Similarly, pathway analysis revealed upregulation of gene ontologies involved in negative regulation of cell-cycle phase transition (GO:0045786 and GO:0010948), apoptosis (R-HSA-109581, GO:0042981), programmed cell death (R-HSA-5357801), intrinsic apoptotic signaling (GO:0008630) and downregulation of signal transduction (GO:0009966), TCR signaling (cd8tcrpathway), response to endogenous stimulus (GO:0009719), mTOR signaling (hsa04150), and response to hypoxia (GO:0001666) pathways in *Cd47*$^{-/-}$ NK cells from tumor-bearing mice (Supplementary Fig. S7). These data suggest a globally impaired NK cell immune response in B16 melanoma–bearing *Cd47*$^{-/-}$ mice.

Discussion

Cytotoxic NK cells are key effectors in cancer immune surveillance, transplantation rejection, and viral immunity (48). TCGA data identified positive correlations for CD47 expression with patient survival and enrichment of NK cell activation markers. Among the cancers analyzed, these correlations are unique to melanomas. Using mouse models and antibody blockade, we identified positive and negative roles for CD47 in regulating NK cell recruitment, activation, proliferation, and survival in the tumor microenvironment. CD47 in NK cells is a cell-intrinsic inhibitory signaling receptor for thrombospondin-1 that limits NK proliferation and activation, consistent with the known CD47-dependent inhibitory functions of thrombospondin-1 in T cells and vascular cells (8, 30). Thrombospondin-1 inhibits TCR-induced proliferation and CD69 induction in a CD47-dependent manner in T cells (8, 30) and inhibited LPS-induced Ki-67 and CD69 expression in NK cells. Treatment with a CD47 blocking antibody reversed thrombospondin-1 inhibition in a human NK cell line, inhibited tumor growth in mice bearing B16 melanoma, and increased tumoral NK cell recruitment and expression of GzmB and IFNγ.

Conversely, we observed a CD47-dependent increase of exhaustion markers in splenic NK cells of melanoma tumor-bearing mice. Immune cell exhaustion has been associated with chronic infection and cancer (49, 50), and sustained infection and tumor growth may lead to NK cell exhaustion (48, 51–55). Downregulation of NK-activating receptors, including NKG2D, CD16, CD146, and NCRs and/or upregulation of certain NK inhibitory receptors such as PD-1, LAG3, TIM-3, or TIGIT are hallmarks of NK cell exhaustion (56). The activating receptor NKG2D is frequently downregulated on NK cells in patients with cancer as well as chronic virus-infected patients (27, 57). Similarly, the inhibitory receptor Tim-3 was upregulated in patients with cancer and chronic hepatitis B and significantly decreased cytotoxicity of peripheral NK cells (58, 59). The cytokine-inducible SH2-containing protein (CIS) has been identified as a critical negative regulator in NK-mediated tumor immunity (60). CIS is a key suppressor of IL15 signaling, promoting NK cell death and limiting proliferation, IFNγ production, and cytotoxicity toward B16 melanoma (60). Similarly, *Mmp9* mediates NK cell dysfunction and augments tumor resistance to NK cytotoxicity within the tumor microenvironment (61, 62). Phenotypic changes and altered expression of these genes consistent with NK exhaustion and dysfunction were found in CD47-deficient NK cells isolated from the spleen of B16-bearing mice, indicating that CD47 systemically protects NK cells from exhaustion. However, our data do not exclude additional contributions of previously reported altered angiogenic and adaptive immune functions in *Cd47*-deficient mice to the faster growth of B16 tumors.

CD47 regulates NK cell transcriptional responses to activating stimuli, and its absence results in a defect in mitochondrial metabolism. CD47 is a known regulator of mitochondrial homeostasis and metabolism (32, 37). Consistent with those studies, *Cd47*$^{-/-}$ NK cells exhibit an increased spare respiratory capacity. The increased mitochondrial proton leak in NK cells and increased intracellular ROS production in *Cd47*$^{-/-}$ NK cells subjected to mitochondrial stress is consistent with the observed apoptotic phenotype. Induction of apoptosis in cytotoxic NK cells after activation is an essential mechanism to prevent autoimmunity (63–65). Mitochondria release proapoptotic factors including ROS and cytochrome-c that activate apoptosis programs in cytolytic lymphocytes, CD8 T cells, and NK cells during the contraction phase (66–68). A resulting systemic depletion of NK cells in *Cd47*$^{-/-}$ mice may contribute to the augmented chronic LCMV infection (11) and B16 melanoma growth. Thus, CD47 has a cell-intrinsic protective function in NK cells that sustains their survival under chronic stress conditions.

Integrins regulated by CD47 play positive roles in T-cell migration and in immune synapse formation (69). Further studies are required to delineate whether defective integrin activation contributes to the impaired NK responses to B16 melanoma in *Cd47*$^{-/-}$ mice. Integrin signaling also limits apoptosis, which could contribute to the apoptotic signature of *Cd47*$^{-/-}$ NK cells in challenged mice (70). Although the absence of CD47 enhances mature NK cell numbers in naïve mice (11), the increased apoptotic signature in challenged mice could result in surface markers that, in the absence of a CD47 don't-eat-me signal, could lead to increased phagocytic clearance of *Cd47*$^{-/-}$ NK cells.

Gene set enrichment suggests that CD47 mediates distinct effects on gene expression in naïve, effector, and memory NK cells. Furthermore, because all immune cell types express CD47, we do not expect that NK cells exclusively mediate the observed functions of CD47 in the tumor microenvironment that regulate melanoma growth.

Our findings have implications for the ongoing clinical development of humanized CD47 antibodies and other biologics that target CD47. Most of the preclinical tumor models supporting these trials were performed using xenogeneic NOD/SCID mice that lack T and B cells but have NK cells and macrophages. Unlike macrophages, NK cells do not express SIRPα but express more CD47 than other lymphocytes (11). If these experimental therapeutics also disrupt the thrombospondin-1-CD47 interaction, they might promote the antitumor activity of NK cells. CD47 antibody treatment could thereby promote activation of systemic and tumor-associated NK cells. The resulting enhanced

production of GzmB and IFNγ by tumor-infiltrating NK cells could contribute to the antitumor efficacy of experimental CD47 therapeutics by increasing direct NK cytotoxicity in addition to the known effects on tumor-associated macrophages.

In summary, these results identify important roles of CD47 in NK cell immune responses to human and murine melanomas. Some of the observed regulation of NK cell activities involves CD47 functioning as an inhibitory signaling receptor for thrombospondin-1, but additional CD47 signaling in NK cells may be mediated by its lateral interactions with integrins and other signaling receptors. Given the essential role of NK cells in tumor immunity, additional studies are needed to define how experimental therapeutics affect CD47–SIRPα versus thrombospondin-1–CD47 signaling in NK cells and to assess their direct effects on antitumor activities of NK cells. Understanding how CD47 signaling in NK cells affects tumor cell killing when combined with cytotoxic or targeted agents may lead to more effective application of these therapeutics.

Disclosure of Potential Conflicts of Interest

A.L. Schwartz is Chief Executive Officer at and has ownership interest (including patents) in Morphiex Biotherapeutics. No potential conflicts of interest were disclosed by the other authors.

Authors' Contributions

Conception and design: P.R. Nath, A.L. Schwartz, D.D. Roberts
Development of methodology: P.R. Nath, D. Pal-Nath, A.L. Schwartz
Acquisition of data (provided animals, acquired and managed patients, provided facilities, etc.): P.R. Nath, A.L. Schwartz
Analysis and interpretation of data (e.g., statistical analysis, biostatistics, computational analysis): P.R. Nath, D. Pal-Nath, A. Mandal, M.C. Cam, A.L. Schwartz, D.D. Roberts
Writing, review, and/or revision of the manuscript: P.R. Nath, D. Pal-Nath, M.C. Cam, A.L. Schwartz, D.D. Roberts
Study supervision: D.D. Roberts
Other (bioinformatic data analysis): A. Mandal

Acknowledgments

The authors thank Dr. Ferenc Livak in the NCI flow cytometry core for assisting with cell analysis and sorting. The authors thank the Office of Science and Technology Resources sequencing facility for performing RNA sequencing. The authors also thank Mr. John M. Sipes for technical support and the rest of the members of Roberts lab for valuable discussions. This work was supported by the Intramural Research Program of the NCI (D.D. Roberts).

The costs of publication of this article were defrayed in part by the payment of page charges. This article must therefore be hereby marked *advertisement* in accordance with 18 U.S.C. Section 1734 solely to indicate this fact.

Received June 5, 2018; revised March 29, 2019; accepted July 26, 2019; published first July 30, 2019.

References

1. Barclay AN, Van den Berg TK. The interaction between signal regulatory protein alpha (SIRPalpha) and CD47: structure, function, and therapeutic target. Annu Rev Immunol 2014;32:25–50.
2. Oldenborg P, Zheleznyak A, Fang Y, Lagenaur CF, Gresham HD, Lindberg FP. Role of CD47 as a marker of self on red blood cells. Science 2000;288:2051–4.
3. Soto-Pantoja DR, Kaur S, Roberts DD. CD47 signaling pathways controlling cellular differentiation and responses to stress. Crit Rev Biochem Mol Biol 2015;50:212–30.
4. Matlung HL, Szilagyi K, Barclay NA, van den Berg TK. The CD47-SIRPalpha signaling axis as an innate immune checkpoint in cancer. Immunol Rev 2017;276:145–64.
5. Kwong LS, Brown MH, Barclay AN, Hatherley D. Signal-regulatory protein alpha from the NOD mouse binds human CD47 with an exceptionally high affinity – implications for engraftment of human cells. Immunology 2014;143:61–7.
6. Soto-Pantoja DR, Terabe M, Ghosh A, Ridnour LA, DeGraff WG, Wink DA, et al. CD47 in the tumor microenvironment limits cooperation between antitumor T-cell immunity and radiotherapy. Cancer Res 2014;74:6771–83.
7. Sockolosky JT, Dougan M, Ingram JR, Ho CC, Kauke MJ, Almo SC, et al. Durable antitumor responses to CD47 blockade require adaptive immune stimulation. Proc Natl Acad Sci U S A 2016;113:E2646–54.
8. Miller TW, Kaur S, Ivins-O'Keefe K, Roberts DD. Thrombospondin-1 is a CD47-dependent endogenous inhibitor of hydrogen sulfide signaling in T cell activation. Matrix Biol 2013;32:316–24.
9. Kaur S, Kuznetsova SA, Pendrak ML, Sipes JM, Romeo MJ, Li Z, et al. Heparan sulfate modification of the transmembrane receptor CD47 is necessary for inhibition of T cell receptor signaling by thrombospondin-1. J Biol Chem 2011;286:14991–5002.
10. Weng TY, Huang SS, Yen MC, Lin CC, Chen YL, Lin CM, et al. A novel cancer therapeutic using thrombospondin 1 in dendritic cells. Mol Ther 2014;22:292–302.
11. Nath PR, Gangaplara A, Pal-Nath D, Mandal A, Maric D, Sipes JM, et al. CD47 expression in natural killer cells regulates homeostasis and modulates immune response to lymphocytic choriomeningitis virus. Front Immunol 2018;9:2985.
12. Spits H, Bernink JH, Lanier L. NK cells and type 1 innate lymphoid cells: partners in host defense. Nat Immunol 2016;17:758–64.
13. Arnon TI, Achdout H, Lieberman N, Gazit R, Gonen-Gross T, Katz G, et al. The mechanisms controlling the recognition of tumor- and virus-infected cells by NKp46. Blood 2004;103:664–72.
14. Halfteck GG, Elboim M, Gur C, Achdout H, Ghadially H, Mandelboim O. Enhanced in vivo growth of lymphoma tumors in the absence of the NK-activating receptor NKp46/NCR1. J Immunol 2009;182:2221–30.
15. Pegram HJ, Andrews DM, Smyth MJ, Darcy PK, Kershaw MH. Activating and inhibitory receptors of natural killer cells. Immunol Cell Biol 2011;89:216–24.
16. Trowsdale J. Genetic and functional relationships between MHC and NK receptor genes. Immunity 2001;15:363–74.
17. Orr MT, Lanier LL. Natural killer cell education and tolerance. Cell 2010;142:847–56.
18. Anfossi N, Andre P, Guia S, Falk CS, Roetynck S, Stewart CA, et al. Human NK cell education by inhibitory receptors for MHC class I. Immunity 2006;25:331–42.
19. Saunders PM, Vivian JP, O'Connor GM, Sullivan LC, Pymm P, Rossjohn J. A bird's eye view of NK cell receptor interactions with their MHC class I ligands. Immunol Rev 2015;267:148–66.
20. Pierson BA, Gupta K, Hu WS, Miller JS. Human natural killer cell expansion is regulated by thrombospondin-mediated activation of transforming growth factor-beta 1 and independent accessory cell-derived contact and soluble factors. Blood 1996;87:180–9.
21. Legrand N, Huntington ND, Nagasawa M, Bakker AQ, Schotte R, Strick-Marchand H, et al. Functional CD47/signal regulatory protein alpha (SIRP(alpha)) interaction is required for optimal human T- and natural killer- (NK) cell homeostasis in vivo. Proc Natl Acad Sci U S A 2011;108:13224–9.
22. Kim MJ, Lee JC, Lee JJ, Kim S, Lee SG, Park SW, et al. Association of CD47 with natural killer cell-mediated cytotoxicity of head-and-neck squamous cell carcinoma lines. Tumour Biol 2008;29:28–34.
23. Yanagita T, Murata Y, Tanaka D, Motegi SI, Arai E, Daniwijaya EW, et al. Anti-SIRPalpha antibodies as a potential new tool for cancer immunotherapy. JCI Insight 2017;2:e89140.
24. Chao MP, Weissman IL, Majeti R. The CD47-SIRPalpha pathway in cancer immune evasion and potential therapeutic implications. Curr Opin Immunol 2012;24:225–32.
25. Willingham SB, Volkmer JP, Gentles AJ, Sahoo D, Dalerba P, Mitra SS, et al. The CD47-signal regulatory protein alpha (SIRPa) interaction is a

therapeutic target for human solid tumors. Proc Natl Acad Sci U S A 2012; 109:6662–7.
26. Majeti R, Chao MP, Alizadeh AA, Pang WW, Jaiswal S, Gibbs KD Jr., et al. CD47 is an adverse prognostic factor and therapeutic antibody target on human acute myeloid leukemia stem cells. Cell 2009;138:286–99.
27. Bezman NA, Kim CC, Sun JC, Min-Oo G, Hendricks DW, Kamimura Y, et al. Molecular definition of the identity and activation of natural killer cells. Nat Immunol 2012;13:1000–9.
28. Gao Q, Chen K, Gao L, Zheng Y, Yang YG. Thrombospondin-1 signaling through CD47 inhibits cell cycle progression and induces senescence in endothelial cells. Cell Death Dis 2016;7:e2368.
29. Kaur S, Chang T, Singh SP, Lim L, Mannan P, Garfield SH, et al. CD47 signaling regulates the immunosuppressive activity of VEGF in T cells. J Immunol 2014;193:3914–24.
30. Kaur S, Martin-Manso G, Pendrak ML, Garfield SH, Isenberg JS, Roberts DD. Thrombospondin-1 inhibits VEGF receptor-2 signaling by disrupting its association with CD47. J Biol Chem 2010;285:38923–32.
31. Kaur S, Soto-Pantoja DR, Stein EV, Liu C, Elkahloun AG, Pendrak ML, et al. Thrombospondin-1 signaling through CD47 inhibits self-renewal by regulating c-Myc and other stem cell transcription factors. Sci Rep 2013; 3:1673.
32. Miller TW, Soto-Pantoja DR, Schwartz AL, Sipes JM, DeGraff WG, Ridnour LA, et al. CD47 receptor globally regulates metabolic pathways that control resistance to ionizing radiation. J Biol Chem 2015;290:24858–74.
33. Li Z, He L, Wilson KE, Roberts DD. Thrombospondin-1 inhibits TCR-mediated T lymphocyte early activation. J Immunol 2001;166:2427–36.
34. Soto-Pantoja DR, Shih HB, Maxhimer JB, Cook KL, Ghosh A, Isenberg JS, et al. Thrombospondin-1 and CD47 signaling regulate healing of thermal injury in mice. Matrix Biol 2014;37:25–34.
35. Lamy L, Ticchioni M, Rouquette-Jazdanian AK, Samson M, Deckert M, Greenberg AH, et al. CD47 and the 19 kDa interacting protein-3 (BNIP3) in T cell apoptosis. J Biol Chem 2003;278:23915–21.
36. Bras M, Yuste VJ, Roue G, Barbier S, Sancho P, Virely C, et al. Drp1 mediates caspase-independent type III cell death in normal and leukemic cells. Mol Cell Biol 2007;27:7073–88.
37. Frazier EP, Isenberg JS, Shiva S, Zhao L, Schlesinger P, Dimitry J, et al. Age-dependent regulation of skeletal muscle mitochondria by the thrombospondin-1 receptor CD47. Matrix Biol 2011;30:154–61.
38. Green DR, Galluzzi L, Kroemer G. Cell biology. Metabolic control of cell death. Science 2014;345:1250256.
39. Maxhimer JB, Soto-Pantoja DR, Ridnour LA, Shih HB, Degraff WG, Tsokos M, et al. Radioprotection in normal tissue and delayed tumor growth by blockade of CD47 signaling. Sci Transl Med 2009;1:3ra7.
40. Seliger B, Wollscheid U, Momburg F, Blankenstein T, Huber C. Characterization of the major histocompatibility complex class I deficiencies in B16 melanoma cells. Cancer Res 2001;61:1095–9.
41. Simonetta F, Pradier A, Roosnek E. T-bet and eomesodermin in NK cell development, maturation, and function. Front Immunol 2016;7:241.
42. Gill S, Vasey AE, De Souza A, Baker J, Smith AT, Kohrt HE, et al. Rapid development of exhaustion and down-regulation of eomesodermin limit the antitumor activity of adoptively transferred murine natural killer cells. Blood 2012;119:5758–68.
43. Gasteiger G, Hemmers S, Bos PD, Sun JC, Rudensky AY. IL-2-dependent adaptive control of NK cell homeostasis. J Exp Med 2013;210:1179–87.
44. Kamimura Y, Lanier LL.Homeostatic control of memory cell progenitors in the natural killer cell lineage. Cell Rep 2015;10:280–91.
45. Beldi-Ferchiou A, Lambert M, Dogniaux S, Vély F, Vivier E, Olive D, et al. PD-1 mediates functional exhaustion of activated NK cells in patients with Kaposi sarcoma. Oncotarget 2016;7:72961–77.
46. Fuertes MB, Iraolagoitia XLR, Ziblat A, Nuñez SY, Torres NI, Secchiari F, et al. Tumor-experienced human NK cells express PD-L1 and display immunoregulatory functions. J Immunol 2017;198 Suppl 1:56.2.
47. Pesce S, Greppi M, Tabellini G, Rampinelli F, Parolini S, Olive D, et al. Identification of a subset of human natural killer cells expressing high levels of programmed death 1: a phenotypic and functional characterization. J Allergy Clin Immunol 2017;139:335–46.
48. Vivier E, Tomasello E, Baratin M, Walzer T, Ugolini S. Functions of natural killer cells. Nat Immunol 2008;9:503–10.
49. Wherry EJ. T cell exhaustion. Nat Immunol 2011;131:492–9.
50. Joyce JA, Fearon DT. T cell exclusion, immune privilege, and the tumor microenvironment. Science 2015;348:74–80.
51. Herberman RB, Nunn ME, Holden HT, Larvin DH. Natural cytotoxic reactivity of mouse lymphoid cells against syngeneic and allogeneic tumors. II. Characterization of effector cells. Int J Cancer 1975;16: 230–9.
52. Kiessling R, Klein E, Wigzell H. "Natural" killer cells in the mouse. I. Cytotoxic cells with specificity for mouse Moloney leukemia cells. Specificity and distribution according to genotype. Eur J Immunol 1975;5: 112–7.
53. Vivier E, Ugolini S, Blaise D, Chabannon C, Brossay L. Targeting natural killer cells and natural killer T cells in cancer. Nat Rev Immunol 2012;12: 239–52.
54. Alvarez-Breckenridge CA, Yu J, Price R, Wojton J, Pradarelli J, Mao H, et al. NK cells impede glioblastoma virotherapy through NKp30 and NKp46 natural cytotoxicity receptors. Nat Med 2012;18:1827–34.
55. Guillerey C, Ferrari de Andrade L, Vuckovic S, Miles K, Ngiow SF, Yong MC, et al. Immunosurveillance and therapy of multiple myeloma are CD226 dependent. J Clin Invest 2015;125:2077–89.
56. Kared H, Martelli S, Tan SW, Simoni Y, Chong ML, Yap SH, et al. Adaptive NKG2C+CD57+ natural killer cell and tim-3 expression during viral infections. Front Immunol 2018;9:686.
57. Mamessier E, Sylvain A, Thibult ML, Houvenaeghel G, Jacquemier J, Castellano R, et al. Human breast cancer cells enhance self tolerance by promoting evasion from NK cell antitumor immunity. J Clin Invest 2011; 121:3609–22.
58. Sun C, Xu J, Huang Q, Huang M, Wen H, Zhang C, et al. High NKG2A expression contributes to NK cell exhaustion and predicts a poor prognosis of patients with liver cancer. Oncoimmunology 2017;6:e1264562.
59. Baba N, Van VQ, Wakahara K, Rubio M, Fortin G, Panzini B, et al. CD47 fusion protein targets CD172a+ cells in Crohn's disease and dampens the production of IL-1beta and TNF. J Exp Med 2013;210:1251–63.
60. Delconte RB, Kolesnik TB, Dagley LF, Rautela J, Shi W, Putz EM, et al. CIS is a potent checkpoint in NK cell-mediated tumor immunity. Nat Immunol 2016;17:816–24.
61. Albertsson PA, Basse PH, Hokland M, Goldfarb RH, Nagelkerke JF, Nannmark U, et al. NK cells and the tumour microenvironment: implications for NK-cell function and anti-tumour activity. Trends Immunol 2003;24: 603–9.
62. Fiore E, Fusco C, Romero P, Stamenkovic I. Matrix metalloproteinase 9 (MMP-9/gelatinase B) proteolytically cleaves ICAM-1 and participates in tumor cell resistance to natural killer cell-mediated cytotoxicity. Oncogene 2002;21:5213–23.
63. Daniels KA, Devora G, Lai WC, O'Donnell CL, Bennett M, Welsh RM. Murine cytomegalovirus is regulated by a discrete subset of natural killer cells reactive with monoclonal antibody to Ly49H. J Exp Med 2001;194: 29–44.
64. Dokun AO, Kim S, Smith HR, Kang HS, Chu DT, Yokoyama WM. Specific and nonspecific NK cell activation during virus infection. Nat Immunol 2001;2:951–6.
65. Sun JC, Beilke JN, Lanier LL. Adaptive immune features of natural killer cells. Nature 2009;457:557–61.
66. Min-Oo G, Bezman NA, Madera S, Sun JC, Lanier LL. Proapoptotic Bim regulates antigen-specific NK cell contraction and the generation of the memory NK cell pool after cytomegalovirus infection. J Exp Med 2014;211: 1289–96.
67. Kroemer G, Reed JC.Mitochondrial control of cell death. Nat Med 2000;6: 513–9.
68. Grayson JM, Laniewski NG, Lanier JG, Ahmed R. Mitochondrial potential and reactive oxygen intermediates in antigen-specific CD8+ T cells during viral infection. J Immunol 2003;170:4745–51.
69. Azcutia V, Routledge M, Williams MR, Newton G, Frazier WA, Manica A, et al. CD47 plays a critical role in T-cell recruitment by regulation of LFA-1 and VLA-4 integrin adhesive functions. Mol Biol Cell 2013;24: 3358–68.
70. Streuli CH. Integrins and cell-fate determination. J Cell Sci 2009;122: 171–7.